# Effects of Dynamic Lattice Distortions on the Structure of the $F$ Band in the Cesium Halides*

P. R. MORAN†
*Department of Physics and Materials Research Laboratory, University of Illinois, Urbana, Illinois*
(Received 21 August 1964)

The smooth, nearly Gaussian, optical absorption band of $F$ centers in most alkali halides contrasts with that observed at low temperatures in the cesium halides, where two or sometimes three components are partially resolved. A strong spin-orbit coupling could account for two components, but the third has remained a mystery because of the cubic symmetry of the alkali-halide lattice. The calculations of this paper show that the cesium halide $F$-band structure can be explained by the instantaneous distortion of the $F$ center's environment from cubic symmetry induced by the motion of the lattice. We calculate the optical absorption line shapes and the low-temperature magneto-optic properties of the $F$ center by using perturbation theory to describe the noncubic electron-vibrational interactions in the limit of strong spin-orbit coupling and by using the Franck–Condon approximation to treat the distribution of vibrational distortions of both cubic and noncubic symmetry. The approximate line shapes obtained have three components corresponding to the three excited state Kramers doublets and can be brought into good agreement with the experimental results for CsI, CsBr, CsCl, and CsF by a suitable choice of the interaction parameters for each material. The same parameters satisfactorily account for the observed circular dichroism and Faraday rotation. A qualitative explanation of the effect of changing the halogen is given in terms of the physical properties of the halogen ions and the manner in which their motion diminishes the cubic interactions and enhances the noncubic interactions. The influence of the temperature upon the structure is also discussed. The different relative strengths of the various interactions account for the striking contrast between the cesium-halide $F$ bands and those observed in the salts which have a relatively light alkali.

## I. INTRODUCTION

IT is well known that the $F$-center optical absorption is a smooth, nearly Gaussian band in those alkali halides in which the ions are of relatively small atomic number. In these salts, the single-configuration-coordinate model of the electron-vibrational interaction[1] has been successful in giving a reasonable fit to the experimental results as shown most recently, for example, by the work of Klick, Patterson, and Knox[2] on the KCl $F$ band. Similar success, however, is utterly lacking for the cesium halide $F$-center absorption where one observes a structured optical band at low temperatures[3–6] as indicated in Fig. 1 for CsI, CsBr, and CsCl. That this structure is due neither to a static asymmetry in the center's environment nor to some peculiarity of the simple cubic CsCl lattice has been demonstrated by the experiments of Hughes and Allard,[7] Lynch,[5] Fitchen,[8] and Hughes and Rabin.[6] In fact, in CsF which has the normal fcc lattice, the $F$ band exhibits three components even more well resolved than in CsCl. The CsF results of Hughes and Rabin are reproduced in Fig. 2. Tentative speculation that part of the structure results from a large spin-orbit splitting was discouraged by the calculations of Suffczynski[9] which predicted the spin-orbit coupling to be about five orders of magnitude too small. Recent magneto-optic studies,[10,11] however, indicate that the spin-orbit splitting is actually quite large and, in particular, the circular dichroism experiments of Margerie and Romestain[12] on CsBr and CsCl and the Faraday effect results of Mort, Lüty, and Brown[13] for CsBr show the spin-orbit coupling to be nearly sufficient to explain the resolution of two of the components. Smith[14] has explained both the magnitude and inverted sense of the coupling by treating the large current "backflow" near neighboring ions produced by orthogonalizing the $F$-center states to the ionic core functions.

Both theory[15] and experiment[16] strongly suggest that the excited state of the $F$-band transition is, in Bethe's notation,[17] a $\Gamma_4$ orbital triplet analogous to the $2P$ level

* This work was supported in part by the U. S. Atomic Energy Commission under contract AT(11-1)-1198.
† National Science Foundation Postdoctoral Fellow.
[1] An excellent review of the methods and approximations used to treat the effects of lattice vibrations upon optical transitions in solids is given by D. L. Dexter, in *Solid State Physics,* edited by F. Seitz and D. Turnbull (Academic Press Inc., New York, 1963), Vol. 6; J. J. Markham, Rev. Mod. Phys. **31**, 956 (1959); and more recently regarding the general question of many-phonon processes by Yu. E. Perlin, Usp. Fiz. Nauk **80**, 553 (1963) [English transl.: Soviet Phys.—Uspekhi **6**, 542 (1964)].
[2] C. C. Klick, D. A. Patterson, and R. S. Knox, Phys. Rev. **133**, A1717 (1964).
[3] H. Rabin and J. H. Schulman, Phys. Rev. Letters **4**, 280 (1960); Phys. Rev. **125**, 1584 (1962).
[4] R. Avakain and A. Smakula, Bull. Am. Phys. Soc. **5**, 48 (1960).
[5] D. W. Lynch, Phys. Rev. **127**, 1537 (1962). The cesium iodide data of Fig. 1 were provided in a private communication.
[6] F. Hughes and H. Rabin, Chem. Phys. Solids **24**, 586 (1963).
[7] F. Hughes and J. G. Allard, Phys. Rev. **125**, 173 (1961).
[8] D. B. Fitchen, Phys. Rev. **133**, A1599 (1964).
[9] M. Suffczynski, J. Chem. Phys. **38**, 1558 (1963). These results prompted a search for alternative explanations such as, for example, those discussed by R. S. Knox, Phys. Rev. **133**, A498 (1964).
[10] F. Lüty and J. Mort, Phys. Rev. Letters **12**, 45 (1964).
[11] N. V. Karlov, J. Margerie, and Y. Merle-D'Aubigné, J. Phys. **24**, 717 (1963).
[12] J. Margerie and R. Romestain, Compt. Rend. **258**, 2525 (1964).
[13] J. Mort, F. Lüty, and F. C. Brown, Phys. Rev. **137**, A566 (1965).
[14] D. Y. Smith, Phys. Rev. **137**, A574 (1965).
[15] See, for example, the article of Barry S. Gourary and Frank J. Adrian, in *Solid State Physics*, edited by F. Seitz and D. Turnbull (Academic Press Inc., New York, 1960), Vol. **11**.
[16] R. H. Silsbee, Phys. Rev. **103**, 1675 (1956).
[17] H. A. Bethe, Ann. Physik **3**, 133 (1929).

of an alkali atom. In a crystal field of cubic symmetry, the spin-orbit interaction splits the levels into a doubly degenerate $\Gamma_6$ and a quadruply degenerate $\Gamma_8$ state. These multiplets are analogous to the $P_{1/2}$ and $P_{3/2}$ levels of an alkali atom and qualitatively account for some of the magneto-optic behavior although they still do not explain the three peaks observed in CsCl and CsF.

The symmetry of the lattice, however, does not determine the instantaneous environment of the $F$ center because lattice vibrations cause the surrounding ions to suffer dynamic distortion from their symmetry positions. This motion produces noncubic potentials which reduce the excited state degeneracy by splitting the $\Gamma_8$ levels to leave only the Kramers doublets. Henry, Schnatterly, and Slichter[18] (HSS) have used the method of moments to analyze the CsBr and CsCl $F$-band circular dichroism. They find that noncubic lattice vibrations can explain the excess $\Gamma_6$–$\Gamma_8$ splitting and the change in relative circular polarization oscillator strengths observed by Margerie and Romestain.[12]

In the present treatment we extend these notions by employing the Franck-Condon approximation to calculate the detailed line shapes and paramagnetic magneto-optic properties of an $F$ center in which the electron undergoes a spin-orbit interaction and vibrational interactions with distortions of both cubic and noncubic symmetry. The results so obtained are not as rigorous as those of a moments calculation, but provide more detailed information. They explicitly demonstrate that the main absorption spectrum of the $F$ center is composed not of two, but of three bands whose degree of resolution depends on the relative strength of the various interactions. A single selection of three interaction parameters determines the over-all breadth of the composite band, the line shape of the individual components, the separation between their peak positions, the behavior of the Faraday effect, and the changes in relative circular polarization oscillator strength of the components from that characterized by the alkali atom. These predicted properties can be brought into good agreement with the experimental data in the cesium halides by a suitable choice of the parameters in each material.

Some of the effects mentioned above can be partially understood in terms of the dynamical properties of the Jahn-Teller effect as treated by Longuet-Higgins, Öpik, Pryce, and Sack.[19] Kristofel' and Zavt,[20] for example, have applied such a treatment to the $^1S_0 \rightarrow {}^3P_1$ transition of KCl:Tl for which, however, no structure is experimentally observed. The complications of a large spin-orbit splitting, nondegenerate vibrational modes, absence of spherical symmetry in a crystal, and threefold orbital degeneracy of the $F$-center excited state

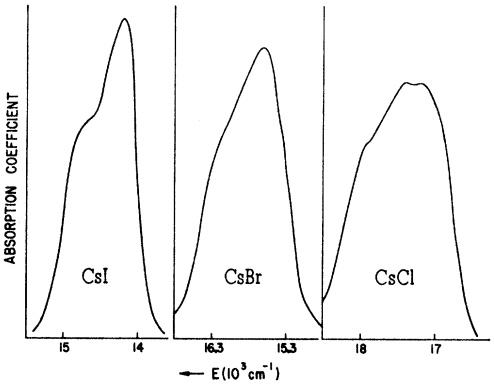


FIG. 1. The $F$-center optical absorption bands at low temperatures in CsI, CsBr, and CsCl.

necessitate that detailed line shapes be obtained by a method other than attempting an approximate solution of the vibronic quantum levels. The treatment of the following sections therefore approaches the problem from a viewpoint different from that employed by the authors mentioned above.

The gross structure resulting from the effects previously discussed is of course different from that observed, for example, in the $R$-center transition by Fitchen, Silsbee, Fulton, and Wolf.[21] The $R$-center structure reflects the discrete quantum levels of the vibrational modes and is shown by Silsbee[22] and McCumber[23] to appear even for singlet-to-singlet transitions in solids. We subsequently refer to the vibrational effects treated in the present work as "dynamic distortion effects" in order to distinguish them from those considered by Silsbee or McCumber and from those of primary concern to Longuet-Higgins *et al.*

Dynamic distortion effects should also be important for other defect and intrinsic absorptions in solids. For example, Knox and Fowler have suggested to the author that such effects could conceivably play a role in the

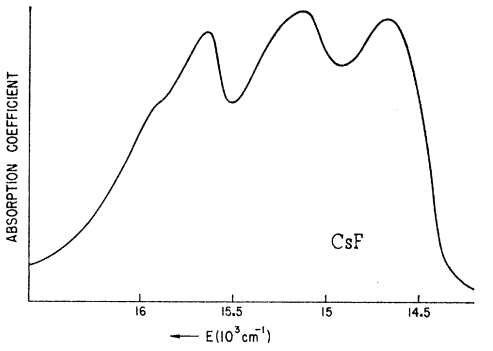


FIG. 2. The $F$-center optical absorption band at low temperature in CsF.

[18] C. H. Henry, S. E. Schnatterly, and C. P. Slichter, Phys. Rev. Letters **13**, 130 (1964), and Phys. Rev. **137**, A602 (1965). These authors are subsequently referred to as HSS.

[19] H. C. Longuet-Higgins, U. Öpik, M. H. L. Pryce, and R. A. Sack, Proc. Roy. Soc. (London) **A244**, 1 (1958).

[20] N. N. Kristofel' and G. S. Zavt, Fiz. Tverd. Tela **5**, 1279 (1963) [English transl.: Soviet Phys.—Solid State **5**, 932 (1963)].

[21] D. B. Fitchen, R. H. Silsbee, T. A. Fulton, and E. L. Wolf, Phys. Rev. Letters **11**, 275 (1963).

[22] R. H. Silsbee, Phys. Rev. **128**, 1726 (1962).

[23] D. E. McCumber, J. Math. Phys. **5**, 221, 508 (1964).

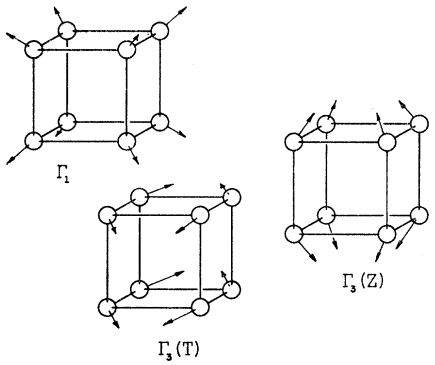


FIG. 3. Displacements of the ions of the nearest neighbor shell for an $F$-center site in the CsCl lattice.

exciton-$F$-center structure correlation noted by Knox in the article mentioned in footnote 9. In the following text, however, we discuss specifically only the $F$-center transition.

This paper is divided into four remaining sections as follows. The model for the $F$-center electron-vibrational and spin-orbit interactions is discussed in Sec. II. These considerations are used in Sec. III to calculate the approximate electronic wave functions and transition probabilities. In Sec. IV, we derive expressions for the unpolarized lineshapes and paramagnetic magneto-optic properties and compare the results with the experimental data for the cesium halides. A discussion of the validity of the approximations used in this treatment is reserved for Sec. V which also contains a qualitative discussion of the variation of the interaction parameters as the halogen ions are changed.

## II. THE $F$-CENTER MODEL

The customary notation for the $F$-center ground state as $S_{1/2}$ levels and the excited state as $P_{1/2}$ and $P_{3/2}$ multiplets is continued here, although this terminology is somewhat imprecise because of the cubic symmetry of the crystal potential. To simplify derivation of the important electron-vibrational interactions, we picture the $F$-center-lattice system as a "quasimolecule" as discussed by Lax.[24] Odd-parity vibrations are ignored because we do not wish to treat higher order effects caused by the mixing of nondegenerate levels. The normal modes of vibration of the neighboring positive ions are found by standard techniques[25] and have the representations $\Gamma_1$, $\Gamma_3$, and $\Gamma_5$. Simple basis functions for these distortions are

$$\Gamma_1: \quad x^2+y^2+z^2, \tag{2.1}$$

$$\Gamma_3: \quad 3z^2-r^2;\ 3^{1/2}(x^2-y^2), \tag{2.2}$$

and

$$\Gamma_5: \quad xy;\ yz;\ zx, \tag{2.3}$$

where two independent sets of the triply degenerate $\Gamma_5$ vibrations exist for the CsCl lattice. To simplify the calculations further, we neglect the $\Gamma_5$ distortions because, although easily included in a more general treatment, their effect upon the primary absorption properties of the cesium halide $F$ centers can be approximated, as discussed in Sec. V, by a modification of the strength of the $\Gamma_3$ interactions. The displacements of the symmetric and the two degenerate tetragonal vibrations are shown in Fig. 3. Lüty and Gebhardt[26] also discuss tetragonal vibrations for the $F$ center, but consider only one of the two modes of this kind.

We denote the $\Gamma_1$ coordinate by $S$ and the $\Gamma_3$ coordinates by $Z$ and $T$ for the $3z^2-r^2$ and the $x^2-y^2$ distortions, respectively. Assuming that electron-vibrational interactions linear in the mode coordinate are dominant, the interaction Hamiltonian can be represented[25] by

$$\mathcal{H}_{eL}'=C_1(x^2+y^2+z^2)S+C_3(3z^2-r^2)Z +C_3 3^{1/2}(x^2-y^2)T. \tag{2.4}$$

Since $S$ is normally measured with respect to its equilibrium position in the lower electronic level, we subtract the symmetric interaction with the electronic ground state from $\mathcal{H}_{eL}'$ and add it to the definition of the zero of the $\Gamma_1$ vibrational Hamiltonian. The matrix elements of the resulting interaction Hamiltonian are then different from zero only for the excited states. We assume that mixing-in of higher lying states by the vibrations may be neglected, and, consequently, we can use a technique familiar in magnetic resonance to express the electrostatic interactions by angular momentum operators,[27] thereby obtaining

$$\mathcal{H}_{eL}=-\gamma_1(\tfrac{1}{2}\mathbf{L}\cdot\mathbf{L})S-\gamma_3(3L_z^2-\mathbf{L}\cdot\mathbf{L})Z -\gamma_3 3^{1/2}(L_x^2-L_y^2)T. \tag{2.5}$$

We can see from this form that the couplings to $Z$ and $T$ are the $F$ center's quadrupole moment interaction with the distortion-induced axial and nonaxial electric field gradients and that the coupling to $S$ is the interaction with changes in the cubic potential induced by breathing mode distortions. We next assume that the total Hamiltonian for this model may be written as the sum of an electron-only term, $\mathcal{H}_e$, a lattice-only term, $\mathcal{H}_L$, and the electron-lattice interaction of Eq. (2.5):

$$\mathcal{H}=\mathcal{H}_e+\mathcal{H}_L+\mathcal{H}_{eL}, \tag{2.6}$$

where $\mathcal{H}_L$ is assumed to be three simple-harmonic-oscillator Hamiltonians of the three vibrational modes.

Even with the simplifications already made a detailed solution of the system wave functions is outside the scope of this paper, and additional approximations are necessary. The first of these is that the electronic wave

[24] M. Lax, J. Chem. Phys. **20**, 1752 (1952).

[25] See, for example, L. Landau and E. Lifshitz, *Quantum Mechanics* (Addison-Wesley Publishing Company, Inc., Reading, Massachusetts, 1958); or V. Heine, *Group Theory in Quantum Mechanics* (Pergamon Press Inc., New York, 1960).

[26] F. Lüty and W. Gebhardt, Z. Physik **169**, 1596 (1963).

[27] Any equivalent representation is, of course, also valid, but the form in Eq. (2.5) is appropriate to the angular-momentum representation employed for the wave functions. A thorough discussion is given in C. P. Slichter, *Principles of Magnetic Resonance* (Harper and Row Inc., New York, 1963), Chap. 6.

functions may be obtained by treating the mode coordinates as classical position coordinates or adiabatic parameters. The second approximation is that the vibrational coordinates do not change during an optical transition and that their distribution may be obtained from the square of the lattice oscillator wave functions for the lower electronic level. The third approximation is that the energy of a particular optical transition is the difference between the adiabatic electronic energies of the upper and lower states. The three preceding approximations are the explicit statement of the semiclassical Franck-Condon approximation as given by Lax[24] and are subsequently referred to as such.[28]

One should note that there are two equivalent viewpoints concerning the changes in the lattice energy during an optical transition. The first is to define a lattice-only Hamiltonian and a separate electron-lattice interaction as in Eq. (2.6). In an optical transition, we then say that the lattice-only energy does not change, and that the spread in energies forming the band comes from changes in the electron-lattice interaction energy. Alternatively, we may include the electron-lattice interaction as part of the lattice energy and define different vibrational Hamiltonians for the upper and lower electronic levels. From the latter viewpoint we may say that the lattice energy changes upon an optical excitation and that the vibrational states immediately after the transition are more or less highly excited. Lax shows the Franck-Condon approximation to be valid when the physical state of the lattice after the absorption process typically corresponds to a high degree of excitation of the vibrational levels for the new effective lattice Hamiltonian of the excited state.

The following section outlines the calculation of the adiabatic wave functions and the absorption probabilities for the various electronic states and conditions of polarization of the incident radiation.

## III. THE ADIABATIC WAVE FUNCTIONS

### The Large Spin-Orbit Limit

The potential energy of the electron-only term of Eq. (2.6) is assumed to be the sum of the static-lattice Coulomb interactions,[15] $\mathcal{H}_0$, and the spin-orbit interaction,[14] $\lambda^*\mathbf{L}\cdot\mathbf{S}$. The effective Hamiltonian for this model is, therefore,

$$\mathcal{H}=\mathcal{H}_0+\lambda^*\mathbf{L}\cdot\mathbf{S}+\mathcal{H}_{eL}+\mathcal{H}_L. \tag{3.1}$$

The energy difference between the ground and first excited states corresponding to $\mathcal{H}_0$ is defined as $\bar{E}$ and, since the energy difference corresponding to the lattice-only term is zero as previously discussed, $\mathcal{H}_L$ is ignored in the following calculations. The $S_{1/2}$ states are written as $|0,M_S\rangle$ and the $P$ multiplets are written as $|J,M_J\rangle$. The excited state Hamiltonian matrix of Eq. (3.1) is

$$\langle J,M_J|\mathcal{H}|J',M_J'\rangle=\begin{array}{c|cccccc|}
 & |\tfrac{3}{2},\tfrac{3}{2}\rangle & |\tfrac{3}{2},-\tfrac{1}{2}\rangle & |\tfrac{1}{2},-\tfrac{1}{2}\rangle & |\tfrac{3}{2},-\tfrac{3}{2}\rangle & |\tfrac{3}{2},\tfrac{1}{2}\rangle & |\tfrac{1}{2},\tfrac{1}{2}\rangle \\
 & \bar{E}+\tfrac{1}{2}\lambda^*+z+s & t & -2^{1/2}t & & & \\
 & t & \bar{E}+\tfrac{1}{2}\lambda^*-z+s & -2^{1/2}z & & & \\
 & -2^{1/2}t & -2^{1/2}z & \bar{E}-\lambda^*+s & & & \\
 & & & & \bar{E}+\tfrac{1}{2}\lambda^*+z+s & t & -2^{1/2}t \\
 & & & & t & \bar{E}+\tfrac{1}{2}\lambda^*-z+s & -2^{1/2}z \\
 & & & & -2^{1/2}t & -2^{1/2}z & \bar{E}-\lambda^*+s
\end{array}, \tag{3.2}$$

where

$$s=-\gamma_1 S;\quad t=-\gamma_3 T;\quad z=-\gamma_3 Z. \tag{3.3}$$

The Kramers degeneracy is immediately apparent from Eq. (3.2), and the three doublets are subsequently denoted by $U_\alpha^{\pm};\alpha=1,2,3$. The convention for the subscript $\alpha$ is that the states are arranged in the order of decreasing energy when $\lambda^*$, $t$, and $z$ are all positive. The

[28] This point is stressed because, for example, Ref. 2 uses a different approximation, also stated to be the Franck-Condon approximation, in which only the potential energy of the lattice-only Hamiltonian is assumed the same before and after the optical transition while the kinetic energy of the lattice is always set equal to zero in the excited state. Because the momentum as well as the position of the ions is conserved during the optical transition in the classical limit, the approximation employed in the present treatment assumes that both the kinetic and potential energies of $\mathcal{H}_L$ are the same before and after the absorption process, A moments calculation shows that the latter approximation at least gives the correct mean energy and second moment of the lineshape whereas that of Ref. 2 gives incorrect values even for a single vibrational mode.

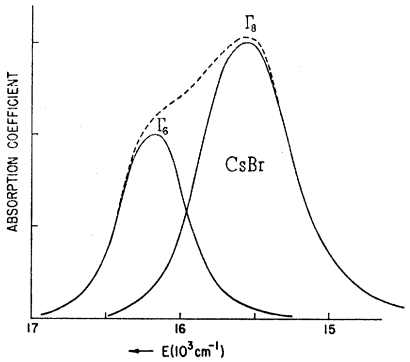


FIG. 4. Decomposition of the CsBr $F$ band into two components corresponding to the broadened $P_{1/2}$ and $P_{3/2}$ multiplets of the alkali atom.

superscript, + or −, refers to the algebraic sign of $M_J$ for the $|M_J|=\frac{3}{2}$ function appearing in that doublet.

To derive approximate line shapes for the $F$ band in the cesium halides, only an approximate diagonalization of the matrix in Eq. (3.2) for the limit of large spin-orbit coupling is required because the cesium halide $F$ centers have values of $|3\lambda^*/2|$ substantially larger than the rms interaction of the electron with the noncubic distortions. Figure 4 shows, as an example, the CsBr $F$ band decomposed by Margerie and Romestain[12] into components roughly identified as the broadened $P_{1/2}$ and $P_{3/2}$ multiplets. That such an identification is at all possible implies that the noncubic interactions must be small relative to the spin-orbit splitting. The adiabatic wave functions are therefore assumed to be adequately described by first diagonalizing the submatrix of the originally degenerate $J=\frac{3}{2}$ state and then treating the noncubic interactions by perturbation theory. The new wave functions are to be calculated to second order in $\lambda^{*-1}$, and the energy corrections found to second order in the theory, i.e., to order $(t^2+z^2)\lambda^{*-1}$. Only one member of each doublet, say $U_\alpha^+$, need be treated explicitly because its magnetic conjugate, $U_\alpha^-$, behaves precisely in the same way. Since the mean energy $\bar{E}$ and the symmetric interaction $s$ are diagonal, they are also temporarily ignored.

## Removal of $\Gamma_8$ Degeneracy

The correct first-order states, $U_1^{+(0)}$ and $U_2^{+(0)}$, are found by diagonalizing the matrix of the degenerate $[|\frac{3}{2},\frac{3}{2}\rangle, |\frac{3}{2},-\frac{1}{2}\rangle]$ pair:

$$\begin{pmatrix} z & t \\ t & -z \end{pmatrix}\begin{pmatrix} a \\ b \end{pmatrix}=\epsilon\begin{pmatrix} a \\ b \end{pmatrix}. \tag{3.4}$$

This equation warrants special consideration because it illustrates the mechanism by which dynamic distortion structure is produced as a result of the "no-crossing" rule for coupled systems. For this simple two-dimensional case, we first consider that only $z$ is a dynamical coordinate of vibrational motion while $t$ is viewed as an external static interaction. Figure 5(A), in which the value of $t$ is zero, shows that the states remain unmixed as $z$ varies, the electron-vibrational adiabatic energy varies linearly with $z$, and the levels cross at $z=0$. The curve labeled $f(z)$ in Fig. 5(A) indicates a typical distribution of $z$, and from it one observes that the most probable value of $z$ is zero and that the most probable value of the splitting, $2|\epsilon|$, is likewise zero. On the other hand, if $t$ has a finite value, say $\frac{1}{2}\Delta E$, as shown in Fig. 5(B), then the energy levels do not cross because the states are mixed by the off-diagonal interaction and are split apart in energy even for small $z$. Although the distribution $f(z)$ still gives a most probable value of zero for $z$, the existence of the coupling term causes the most probable value of the splitting to be $2|\epsilon|_{\min}=\Delta E$.

By including the harmonic potential, $\frac{1}{2}kZ^2$, as well as the electron-vibrational interaction $\epsilon$, the adiabatic potentials shown in Fig. 6 are obtained. The allowed vibrational levels are qualitatively indicated by the horizontal lines drawn within the potential curves. In Fig. 6(A) there is no off-diagonal coupling so that two simple displaced parabolas result for the adiabatic potentials of the $|\frac{3}{2},\frac{3}{2}\rangle$ and $|\frac{3}{2},-\frac{1}{2}\rangle$ vibronic states. When the coupling is present, as illustrated in Fig. 6(B), the no-crossing rule holds for the adiabatic potentials which then split into the two branches indicated in the figure. The validity of using the adiabatic potentials for determining the ionic motion in a situation such as is shown in Fig. 6(B) must be carefully considered because the electronic states depend strongly on the vibrational coordinate and therefore do not commute with the lattice-only Hamiltonian. This is further discussed by HSS. Nevertheless, one may show qualitatively that the vibrational levels tend to "pile up" as they approach the gap and to be pushed out of the adiabatically forbidden region of the potential. This behavior is schematically indicated in Fig. 6(B) and is responsible for the observed dynamic distortion structure. The corresponding two-dimensional adiabatic potential is shown in Fig. 7 and, even if one ignores the dubious validity of employing the adiabatic approxima-

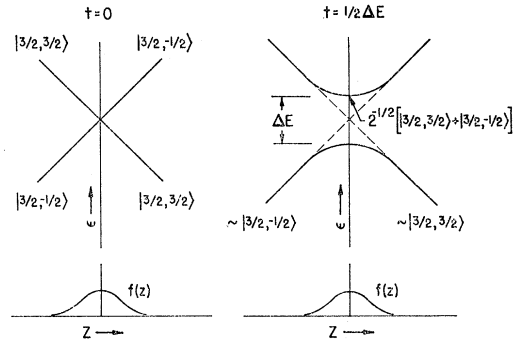


FIG. 5. Schematic representation of the interaction potential of a single vibrational mode with the $P_{3/2}$ states. See discussion given in the text.

tion, the difficulties in determining the detailed behavior of the vibrational states are considerable.

Since our problem, however, is to investigate the more gross features of the absorption spectrum, we now return to finding the adiabatic electronic wave functions. The solution of Eq. (3.4) yields states strongly dependent upon the noncubic distortions;

$$U_1^{+(0)}=a|\tfrac{3}{2},\tfrac{3}{2}\rangle+b|\tfrac{3}{2},-\tfrac{1}{2}\rangle, \tag{3.5}$$

with a splitting $\epsilon_1$ of

$$\epsilon_1=\epsilon\equiv(t^2+z^2)^{1/2}, \tag{3.6}$$

and

$$U_2^{+(0)}=b|\tfrac{3}{2},\tfrac{3}{2}\rangle-a|\tfrac{3}{2},-\tfrac{1}{2}\rangle, \tag{3.7}$$

with a splitting $\epsilon_2$ of

$$\epsilon_2=-\epsilon, \tag{3.8}$$

where

$$a=t[2(t^2+z^2-z\epsilon)]^{-1/2},$$

and

$$b=(\epsilon-z)[2(t^2+z^2-z\epsilon)]^{-1/2}. \tag{3.9}$$

The zero-order state, $U_3^{+(0)}$, is

$$U_3^{+(0)}=|\tfrac{1}{2},-\tfrac{1}{2}\rangle. \tag{3.10}$$

## Transition Probabilities

The functions given above are then used as the starting functions for a perturbation calculation in the interactions $t$ and $z$. The new wave functions, correct to order $\lambda^{*-2}$, and the second-order energies are obtained in a straightforward manner, but the explicit expressions are lengthy and are not reproduced here. The next step is to calculate the square of the optical dipolar matrix elements for circularly polarized light to obtain transition probabilities from the ground states $|0,M_S\rangle$ to the excited states $U_\alpha^+$ and $U_\alpha^-$. Symmetry requires that the noncubic interaction distributions give equal probabilities for the three quantities $z$, $t$, and $(t^2-z^2)$ to have the respective values $|z|$, $|t|$, and $|t^2-z^2|$ or $-|z|$, $-|t|$, and $-|t^2-z^2|$. One achieves considerable simplification by immediately averaging the transition probabilities and energies over $\pm|z|$ and $\pm|(t^2-z^2)|$.

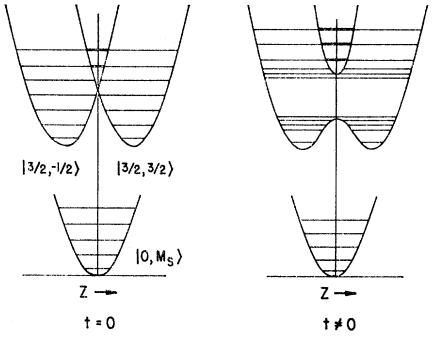


FIG. 6. Vibronic energy levels in the adiabatic potentials of the lower and upper electronic levels. See discussion given in the text.

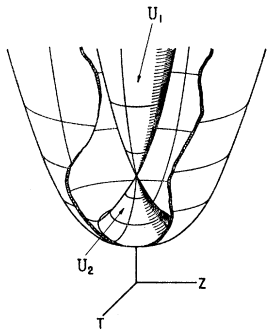


FIG. 7. Adiabatic potential of the two $\Gamma_3$ modes interacting with the $P_{3/2}$ electronic states. The two sheets of the potential are labeled by the corresponding electronic states, $U_1$ and $U_2$.

A small error in the line shapes results from averaging the energies separately from the $U_1$ and $U_2$ transition probabilities, but this is considered negligible compared with the other approximations already employed. The resulting expressions are given in terms of the following notation: $w_\pm(M_S;U_\alpha^\pm)$ is the transition probability for circular polarization, correct to order $(t^2+z^2)(3\lambda^*/2)^{-2}$, from the ground state with spin $M_S$ to the excited state $U_\alpha^\pm$. The subscript of $w$, $+$ or $-$, denotes right or left circular polarization.

One finds the nonzero transition probabilities

$$w_+(\tfrac{1}{2};U_1^+)=w_-(-\tfrac{1}{2};U_1^-)=K\tfrac{1}{2}\{(\tfrac{1}{3})+2z^2(3\lambda^*/2)^{-2}\}, \tag{3.11a}$$

$$w_-(\tfrac{1}{2};U_1^+)=w_+(-\tfrac{1}{2};U_1^-)=K\tfrac{1}{2}\{1-2t^2(3\lambda^*/2)^{-2}\}, \tag{3.11b}$$

at an energy

$$E_1=\bar{E}+\tfrac{1}{2}\lambda^*+s+(t^2+z^2)^{1/2}+(t^2+z^2)(3\lambda^*/2)^{-1}; \tag{3.11c}$$

$$w_+(\tfrac{1}{2};U_2^+)=w_-(-\tfrac{1}{2};U_2^-)=w_+(\tfrac{1}{2};U_1^+), \tag{3.12a}$$

$$w_-(\tfrac{1}{2};U_2^+)=w_+(-\tfrac{1}{2};U_2^-)=w_-(\tfrac{1}{2};U_1^+), \tag{3.12b}$$

at an energy

$$E_2=\bar{E}+\tfrac{1}{2}\lambda^*+s-(t^2+z^2)^{1/2}+(t^2+z^2)(3\lambda^*/2)^{-1}; \tag{3.12c}$$

$$w_+(\tfrac{1}{2};U_3^+)=w_-(-\tfrac{1}{2};U_3^-)=K\tfrac{2}{3}\{1-3z^2(3\lambda^*/2)^{-2}\}, \tag{3.13a}$$

$$w_-(\tfrac{1}{2};U_3^+)=w_+(-\tfrac{1}{2};U_3^-)=K\tfrac{2}{3}\{3t^2(3\lambda^*/2)^{-2}\}, \tag{3.13b}$$

at an energy

$$E_3=\bar{E}-\lambda^*+s-2(t^2+z^2)(3\lambda^*/2)^{-1}. \tag{3.13c}$$

where $K$ is the constant of proportionality. We use the three sets of equations (3.12)–(3.14) in the next section to obtain the approximate $F$-center optical absorption properties.

# IV. $F$-CENTER LINE SHAPE

## Shape Functions

The squares of the zero-point simple harmonic wave functions give Gaussian distributions for the vibrational

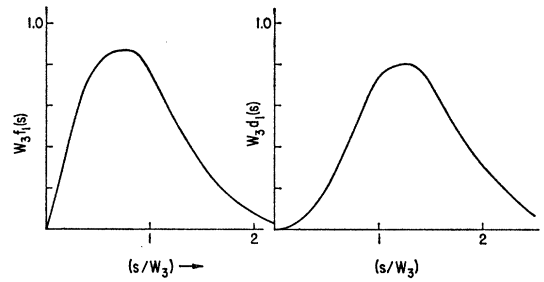


FIG. 8. Characteristics of the tetragonal line-shape functions $f$ and $d$ defined in the text.

interaction elements $s$, $t$, and $z$:

$$P_1(s)=(\pi 2W_1^2)^{-1/2}\exp[-s^2(2W_1^2)^{-1}], \quad (4.1)$$

$$P_3(t)=(\pi W_3^2)^{-1/2}\exp[-t^2W_3^{-2}], \quad (4.2)$$

and

$$P_3(z)=(\pi W_3^2)^{-1/2}\exp[-z^2W_3^{-2}]. \quad (4.3)$$

It can be easily shown that $W_1$ and $W_3$ are the rms interactions with the symmetric and one of the tetragonal distortions, respectively. Using these distributions, the center of gravity shift of the $U_1$ and $U_2$ bands caused by the second-order energy corrections of Eqs. (3.11c) and (3.12c) may be obtained,

$$\langle(t^2+z^2)(3\lambda^*/2)^{-1}\rangle=W_3^2(3\lambda^*/2)^{-1}. \quad (4.4)$$

The second-order energy terms also slightly modify the $U_1$ and $U_2$ line shapes, but for our purposes need only be retained as the center of gravity shift given above. To calculate the spectral transition intensity $p$ we use the energies and transition probabilities of the previous section; for example, the energy $E_1\approx\bar{E}+\frac{1}{2}\lambda^*+W_3^2(3\lambda^*/2)^{-1}+(t^2+z^2)^{1/2}+s=E_1(t,z,s)$, and $w_+(\frac{1}{2},U_1^+;t,z)$ given in Eq. (3.11a) yield

$$p_+(\tfrac{1}{2},U_1^+;E)=\int\int\int P_1(s)P_3(t)P_3(z)w_+(\tfrac{1}{2},U_1^+;t,z)\times\delta[E-E_1(t,z,s)]dsdtdz. \quad (4.5)$$

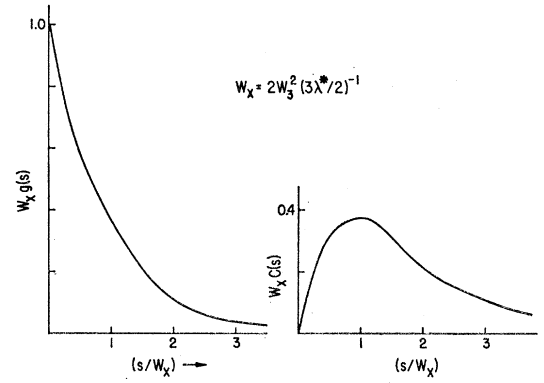


FIG. 9. Characteristics of the tetragonal line-shape functions $g$ and $c$ defined in the text.

This procedure is followed for the various transitions to obtain

$$p_+(\tfrac{1}{2},U_1^+;E)=p_-(-\tfrac{1}{2},U_1^-;E)=K\tfrac{1}{2}\{\tfrac{1}{3}F_1(E)+W_3^2(3\lambda^*/2)^{-2}D_1(E)\}, \quad (4.6a)$$

$$p_+(-\tfrac{1}{2},U_1^-;E)=p_-(\tfrac{1}{2},U_1^+;E)=K\tfrac{1}{2}\{F_1(E)-W_3^2(3\lambda^*/2)^{-2}D_1(E)\}, \quad (4.6b)$$

$$p_+(\tfrac{1}{2},U_2^+;E)=p_-(-\tfrac{1}{2},U_1^-;E)=K\tfrac{1}{2}\{\tfrac{1}{3}F_2(E)+W_3^2(3\lambda^*/2)^{-2}D_2(E)\}, \quad (4.7a)$$

$$p_+(-\tfrac{1}{2},U_2^-;E)=p_-(\tfrac{1}{2},U_1^+;E)=K\tfrac{1}{2}\{F_2(E)-W_3^2(3\lambda^*/2)^{-2}D_2(E)\}, \quad (4.7b)$$

$$p_+(\tfrac{1}{2},U_3^+;E)=p_-(-\tfrac{1}{2},U_3^-;E)=K\tfrac{2}{3}\{G(E)-\tfrac{3}{2}W_3^2(3\lambda^*/2)^{-2}C(E)\}, \quad (4.8a)$$

and

$$p_+(\tfrac{1}{2},U_3^+;E)=p_-(-\tfrac{1}{2},U_3^-;E)=K\tfrac{2}{3}\{\tfrac{3}{2}W_3^2(3\lambda^*/2)^{-2}C(E)\}. \quad (4.8b)$$

The shape functions $F$, $D$, $G$, and $C$ are found to be convolutions of the symmetric broadening with tetragonal-mode-only line shapes; for example,

$$F_{(1,2)}(E)=\int P_1\{[E-(\bar{E}+\tfrac{1}{2}\lambda^*+W_3^2(3\lambda^*/2)^{-1})]-s\}\times f_{(1,2)}(s)ds, \quad (4.9)$$

and

$$G(E)=\int P_1\{[E-(\bar{E}-\lambda^*-2W_3^2(3\lambda^*/2)^{-1})]-s\}\times g(s)ds, \quad (4.10)$$

where $f_1(s)=f_2(-s)$ and $d_1(s)=d_2(-s)$. The noncubic-only line shapes $f_1$, $d_1$, $g$, and $c$ are normalized functions and are shown in Figs. 8 and 9. For the cesium halide $F$ bands, the symmetric broadening dominates, and the final line shapes can be well approximated by the follow-

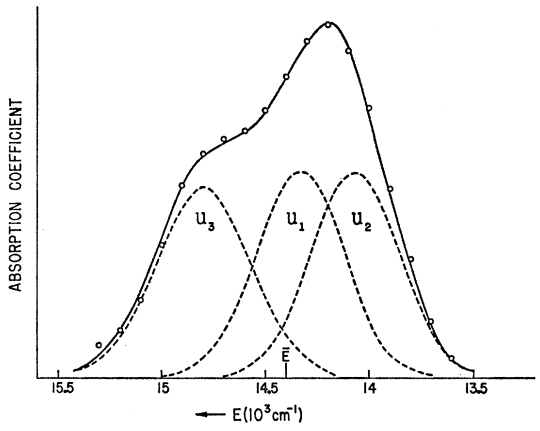


FIG. 10. The dashed curves show the three component bands, $U_1$, $U_2$, and $U_3$, for the values of the parameters $\Delta=465$ cm$^{-1}$, $W_1=210$ cm$^{-1}$, $W_3=140$ cm$^{-1}$, and $\bar{E}=14\,400$ cm$^{-1}$. The solid curve is the corresponding absorption coefficient, and the circles show the experimental results for CsI.

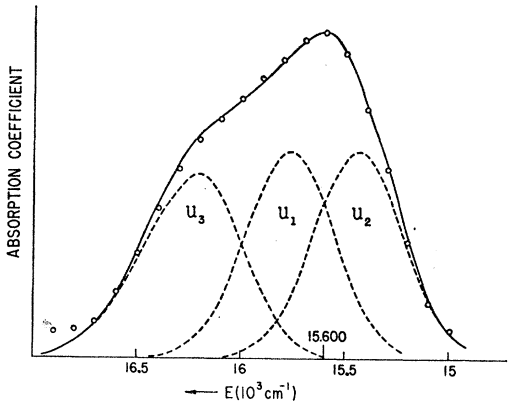


FIG. 11. The curves are the same as indicated in Fig. 10, but here the parameters are $\Delta=420$ cm$^{-1}$, $W_1=200$ cm$^{-1}$, $W_3=180$ cm$^{-1}$, and $\bar{E}=15\,815$ cm$^{-1}$. The circles indicate the experimental results for CsBr.

ing expressions which are constructed to have the same mean energy, second moment about the mean, and approximate asymmetry given by the convolution integrals.

$$F_{(1,2)}\approx\{\pi[2W_1^2+W_f^2]\}^{-1/2}\times\exp\{-[E-(\bar{E}+\tfrac{1}{2}\lambda^*+(3\lambda^*/2)^{-1}W_3^2\pm(\pi/4)^{1/2}W_3)]^2[2W_1^2+W_f^2]^{-1}\},\quad(4.11)$$

where $+(\pi/4)^{1/2}W_3$ and $-(\pi/4)^{1/2}W_3$ are associated with $F_1$ and $F_2$, respectively, and

$$W_f=[\tfrac{1}{2}(4-\pi)]^{1/2}W_3\approx0.65W_3.\quad(4.12)$$

Similarly, associating $\pm(\frac{3}{2})(\pi/4)^{1/2}W_3$ with $D_1$ and $D_2$, respectively, we obtain

$$D_{(1,2)}\approx\{\pi[2W_1^2+W_d^2]\}^{-1/2}\times\exp\{-[E-(\bar{E}+\tfrac{1}{2}\lambda^*+(3\lambda^*/2)^{-1}W_3^2\pm\tfrac{3}{2}(\pi/4)^{1/2}W_3)]^2[2W_1^2+W_d^2]^{-1}\},\quad(4.13)$$

where

$$W_d=[4-(9\pi/8)]^{1/2}W_3\approx0.68W_3.\quad(4.14)$$

The approximate shapes of $G(E)$ and $C(E)$ are given by double Gaussians,

$$G(E)\approx\{[\pi^{1/2}2^{-1/2}(W_1+W_g)]^{-1}\}\times\begin{cases}\exp\{-[E-(\bar{E}-\lambda^*-E_g)]^2(2W_1^2)^{-1}\};\\ \quad\text{for}\quad[E-(\bar{E}-\lambda^*-E_g)]\lambda^{*-1}>0\\ \exp\{-[E-(\bar{E}-\lambda^*-E_g)]^2(2W_g^2)^{-1}\};\\ \quad\text{for}\quad[E-(\bar{E}-\lambda^*-E_g)]\lambda^{*-1}<0,\end{cases}\quad(4.15)$$

where

$$W_g=-W_1[\tfrac{1}{2}(4-\pi)(\pi-2)^{-1}]+2^{-1/2}\pi(\pi-2)^{-1}\times[\tfrac{1}{2}W_1^2+\pi^{-1}(\pi-2)^2W_x^2]^{1/2},\quad(4.16)$$

$$E_g=(\lambda^*/|\lambda^*|)[(\pi/2)^{-1/2}(W_g-W_1)-W_x],\quad(4.17)$$

$$W_x=|2W_3^2(3\lambda^*/2)^{-1}|,\quad(4.18)$$

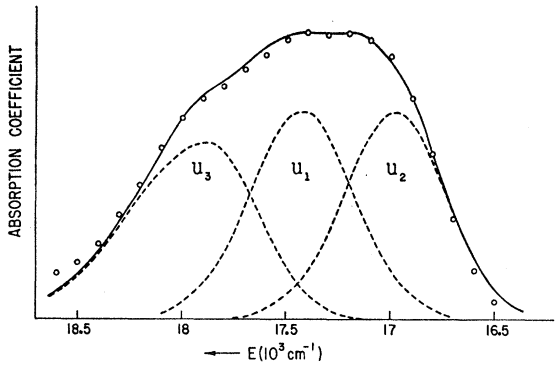


FIG. 12. The curves are the same as indicated in Fig. 10, but here the parameters are $\Delta=420$ cm$^{-1}$, $W_1=240$ cm$^{-1}$, $W_3=230$ cm$^{-1}$, and $\bar{E}=17\,250$ cm$^{-1}$. The circles indicate the experimental results for CsCl.

and

$$C(E)\approx\text{A double-Gaussian distribution obtained from Eqs. (4.15)–(4.17) by everywhere replacing } W_x \text{ with } 2W_x.\quad(4.19)$$

We find the absorption properties by summing the component spectral transition intensities $p$, weighting each according to the population of the $M_S$ level from which it proceeds and the amount of corresponding polarization in the incident radiation. The absorption coefficient $\mu(E)$ is proportional to the total transition intensity multiplied by the transition energy.

### Comparison with Unpolarized Line Shapes

For the $F$ center, $\lambda^*$ is negative[14] and we define $\Delta$ as $-(3\lambda^*/2)$. The experimental absorption is compared in Figs. 10–13 with the unpolarized line shapes obtained from Eqs. (4.6)–(4.8) using the shape functions of Eqs. (4.11)–(4.19).

The circles shown in Fig. 10 are the experimental results of Lynch for the CsI $F$ band. The dashed lines

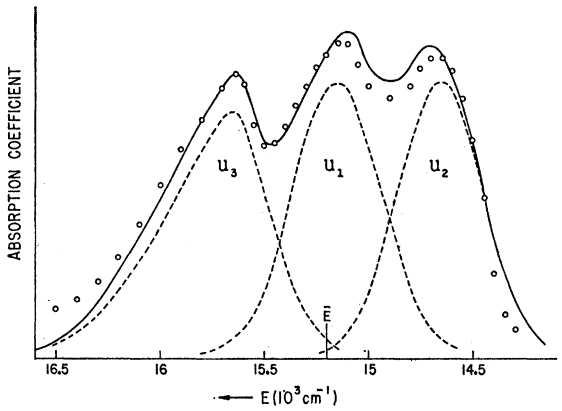


FIG. 13. The curves are the same as indicated in Fig. 10, but here the parameters are $\Delta=400$ cm$^{-1}$, $W_1=175$ cm$^{-1}$, $W_3=260$ cm$^{-1}$, and $\bar{E}=15\,200$ cm$^{-1}$. The circles indicate the experimental results for CsF.

TABLE I. Integrated intensity of the $F$-band components.

| | | $\Gamma_{1g} \rightarrow \Gamma_{6u}$ | | $\Gamma_{1g} \rightarrow \Gamma_{8u}$ | |
|---|---|---|---|---|---|
| | $(W_3/\Delta)$ | $3\int p_-(\frac{1}{2},U_3^+)$ | $3\int p_+(\frac{1}{2},U_3^+)$ | $3\int p_-(\frac{1}{2},U_1^+ + U_2^+)$ | $3\int p_+(\frac{1}{2},U_1^+ + U_2^+)$ |
| *Theoretical* | ... | $3(W_3/\Delta)^2$ | $3[\frac{2}{3}-(W_3/\Delta)^2]$ | $3[1-(W_3/\Delta)^2]$ | $3[\frac{1}{3}+(W_3/\Delta)^2]$ |
| Alkali atom | 0 | 0 | 2 | 3 | 1 |
| CsBr | 0.43 | 0.55 | 1.45 | 2.45 | 1.55 |
| CsCl | 0.52 | 0.80 | 1.20 | 2.20 | 1.80 |
| *Experimental* | | | | | |
| CsBr | ? | 0.5±0.1 | 1.8±0.1 | 2.5±0.1 | 1.2±0.1 |
| CsCl | ? | 0.6±0.1 | 1.6±0.1 | 2.4±0.1 | 1.4±0.1 |

indicate the three components, $p(U_1)$, $p(U_2)$, and $p(U_3)$, for $\Delta=465$ cm$^{-1}$, $W_1=210$ cm$^{-1}$, $W_3=140$ cm$^{-1}$, and $\bar{E}=14\,400$ cm$^{-1}$. The absorption coefficient corresponding to the sum of the $p$'s multiplied by $(E/\bar{E})$ is given by the solid line.

The CsBr $F$-band results of Margerie and Romestain are shown by the circles in Fig. 11. The $U_1$, $U_2$, and $U_3$ bands and the resulting $\mu(E)$ are indicated in the figure for $\Delta=420$ cm$^{-1}$, $W_1=200$ cm$^{-1}$, $W_3=180$ cm$^{-1}$, and $\bar{E}=15\,815$ cm$^{-1}$.

One first observes partial $U_1-U_2$ resolution for $W_3$ just slightly smaller than $W_1$, as shown in the CsCl line shape of Fig. 12. The circles are taken from the results of Rabin and Schulman for the liquid-helium CsCl $F$ band. The theoretical curves are for $\Delta=420$ cm$^{-1}$, $W_1=240$ cm$^{-1}$, $W_3=230$ cm$^{-1}$, and $\bar{E}=17\,250$ cm$^{-1}$.

The well-resolved structure in CsF is indicated by the circles in Fig. 13 taken from the results of Hughes and Rabin. The agreement with the theoretical line shapes for $\Delta=400$ cm$^{-1}$, $W_1=175$ cm$^{-1}$, $W_3=260$ cm$^{-1}$, and $\bar{E}=15\,200$ cm$^{-1}$ is quite remarkable considering the slow convergence of the perturbation expansion with $(W_3/\Delta)=0.65$.

## Temperature Dependence

The preceding results were derived using the zero-point vibrational interaction distributions, but are easily extended to obtain approximate expressions for the absorption properties at finite temperatures by writing $W_1$ and $W_3$ as temperature-dependent parameters according to the usual approximation:

$$W_1(T)=W_1(0)\{\coth[\hbar\omega_1(2kT)^{-1}]\}^{1/2}; \quad (4.20)$$

$$W_3(T)=W_3(0)\{\coth[\hbar\omega_3(2kT)^{-1}]\}^{1/2}. \quad (4.21)$$

The CsCl $F$ band measured by Margerie and Romestain[12] at 1.85°K differs slightly from the helium-temperature results of Rabin and Schulman.[3] An estimate of the temperature effect based on other experimental data and Eqs. (4.20) and (4.21) shows that one might expect about a 5% decrease in the interactions by going to 1.85° and, by reducing $W_3$ to 220 cm$^{-1}$ and $W_1$ to 225 cm$^{-1}$, one indeed obtains agreement with the lower temperature spectrum (not shown) similar to that for the liquid-helium data indicated in Fig. 12. The CsF results of Hughes and Rabin[6] also show quite clearly that both the over-all broadening and the amount of splitting increase with increasing temperature in a manner qualitatively consistent with that obtained from the above equations. Experimental data are, however, insufficient to provide a quantitative test of the predicted temperature dependence.

Temperature effects can perhaps be more readily observed in other systems. For example, the $Pb^{++}$ impurity in NaCl can be reduced by x-ray irradiation to $Pb^0$ and, if the $Pb^+$ impurity can be formed as a stable intermediate impurity, the resulting optical transitions among the spin-orbit levels (parity forbidden in a static lattice) would provide a spectrum free of the over-all broadening caused by the cubic interactions.

## Magneto-Optic Properties

The integrated intensities of the component bands are easily obtained by integrating Eqs. (4.6)–(4.8). Table I lists the theoretical results for CsBr and CsCl, obtained using the parameters previously derived from the unpolarized line shapes, and the experimental values deduced by Margerie and Romestain as given in Ref. 12. Although the agreement between theory and experiment noted in Table I is considered to be quite satisfactory, one may note that those components for which the discrepancies are greatest are the same as those for which the theory predicts the greatest changes in band shape for different polarizations; these components would therefore be the most susceptible to errors in an experimental curve subtraction.

Knowing the shapes and absorption intensities one may also calculate the corresponding paramagnetic Faraday rotation[13] by using the dispersion relations. Employing the parameters given in Fig. 11 and the Smakula relation for the area under the absorption curve, an approximate numerical computation gives the magnitude of the predicted peak paramagnetic Verdet constant for CsBr as

$$\mathcal{V}(\mathrm{CsBr})\big|_{\max}^{\mathrm{para}} \approx (8.6\times10^{-17})(Nf H_0^{-1}) \times\tanh[\beta H_0(kT)^{-1}](\mathrm{G}^{-1}\,\mathrm{cm}^{-1}). \quad (4.22)$$

The value observed by Mort, Lüty, and Brown at 4°K, with a CsBr $F$-center density $Nf=1.1\times10^{17}$ cm$^{-3}$ was $1.2\times10^{-2}$ (deg G$^{-1}$ cm$^{-1}$), while Eq. (4.22) gives the value $0.95\times10^{-2}$ (deg G$^{-1}$ cm$^{-1}$). The difference between the observed and predicted values is within experimental error and, in any event, within the uncertainties due to the computational approximations. In contrast, if one uses the Becquerel relation for Faraday rotation, approximates the maximum derivative of the dispersion curve in terms of the maximum curvature of the absorption band, and relates the characteristic energy shift to the spin-orbit splitting of about 400$^{-1}$, the CsBr Verdet constant predicted for the experimental conditions stated above is nearly a factor of 2 larger than that observed by Mort *et al.*

### Comparison with the Moments Analysis

The rms vibrational interactions used in this treatment to fit the CsBr and CsCl line shapes, circular dichroism, and Faraday effect data are in agreement with the values obtained in the moments analysis of HSS.[18] The moments analysis, however, gives values for the spin-orbit splittings which are about 25% smaller than those used in this paper. Figure 14 shows the experimental line shape for CsBr and the theoretical lineshapes for $\Delta=420$ cm$^{-1}$ and for the HSS value, $\Delta=330$ cm$^{-1}$. Although the former gives a significantly better fit, the latter still gives a line shape which has the same qualitative features and which nowhere differs from the experimental curve by more than 10% of the maximum value. The approximations employed in the present treatment, particularly the assumption $\Delta\gg W_3$, can easily account for the major portion of such differences. Because the difficulties involved in the low temperature circular dichroism measurements are considerable, it may also be possible[29] that some part of the discrepancies noted above is due to systematic experimental error.

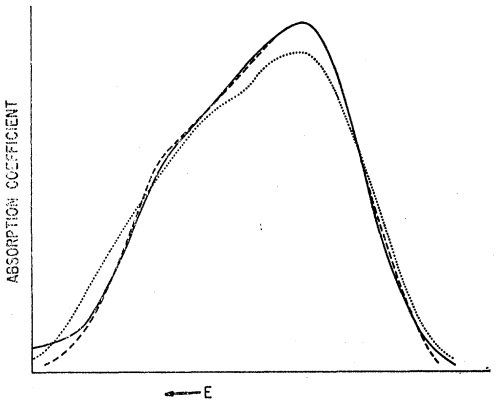


FIG. 14. The solid curve is the experimental absorption coefficient for CsBr $F$ centers. The dashed curve is the theoretical absorption using $\Delta=420$ cm$^{-1}$. The dotted curve is the theoretical absorption using $\Delta=330$ cm$^{-1}$.

## V. DISCUSSION

### Validity of Approximations

With the exception of neglecting distortions of $\Gamma_5$ symmetry, there is sufficient previous experimental evidence[1,30] to indicate that all the model approximations used in this paper provide a description of the $F$-center system which is adequate for the purposes of the present treatment. To investigate the validity of ignoring $\Gamma_5$ vibrations one may carry out a rigorous moments calculation[18,24] including the $\Gamma_5$ interactions, but retaining all other model approximations. It is necessary to go to the fourth moment and changes in the fourth moment induced by external fields[18] before the $\Gamma_5$ interactions appear in a manner other than as a simple additive term to the square of the rms $\Gamma_3$ interactions. All but the Kramers degeneracy has already been removed by the tetragonal distortions, and they alone already produce dynamic distortion structure because of the strong spin-orbit coupling in the cesium halides. The $\Gamma_5$ vibrations can, therefore, only modify the existing line shapes and, because they contribute to the lower moments only in the trivial way noted above, their effect may be included to a good approximation[31] by simply redefining the noncubic parameter $W_3^2$ as

$$(W_3^2)_{\text{effective}}=\tfrac{1}{2}\langle E^2\rangle_3+\tfrac{1}{2}\langle E^2\rangle_5, \qquad (5.1)$$

where $\langle E^2\rangle_3$ and $\langle E^2\rangle_5$ are the squared rms interactions of all the $\Gamma_3$ and $\Gamma_5$ distortions, respectively.

The most important computational approximations are the use of perturbation theory in the large spin-orbit limit and the three assumptions of the Franck-Condon approximation. These may be investigated by comparing the rigorous moments calculations with the results obtained directly from the approximate line shapes. The errors associated with the Franck-Condon approximation can, in this way, be shown to be small when the linewidth is large compared with the typical phonon energies, a condition satisfied in the cesium halide $F$-center system. The most objectionable approximation is the use of perturbation theory which, in the second and higher moments, causes errors whose values are small for the parameters appropriate to CsI, but are about 25% for the parameters used in fitting the CsF results. Consequently, an exact diagonalization of the interaction matrix of Eq. (3.2) would be necessary to reduce the differences between the present treatment

[29] J. Margerie (private communication).

[30] See, for example, W. D. Compton and J. H. Schulman, *Color Centers in Solids* (Pergamon Press Inc., New York, 1962), and, for specific points, I. S. Jacobs, Phys. Rev. **93**, 993 (1954), and J. D. Konitzer and J. J. Markham, J. Chem. Phys. **32**, 843 (1960).

[31] This procedure is not justified for all singlet to multiplet transitions. For example, a $1S\rightarrow 2P$ transition in which there is negligible spin-orbit coupling will be composed of bands split by dynamic distortion effects only if the $\Gamma_5$ as well as the $\Gamma_3$ interactions are present. See Ref. 20 for the analogous $^1S_0\rightarrow{}^3P_1$ transition.

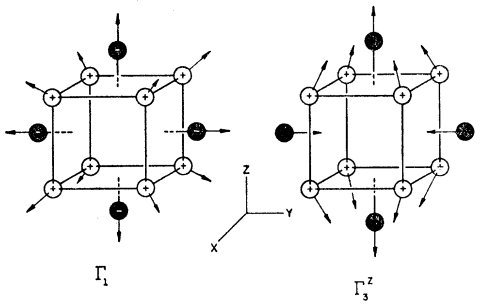


FIG. 15. Displacements of the nearest-neighbor alkali ions and halogen ions about the $F$-center site in a CsCl lattice. See discussion given in the text.

and the experimental results which, at least for the CsF spectrum shown in Fig. 13, are as much as 20–30%.

## Variation of the Interactions

Since the iodine ion is nearly as massive as the cesium ion and, moreover, has about a 35% larger ionic radius, one might expect that, for CsI the halogen shells are, in a sense, locked in place and do not participate in the low-frequency vibrational motion to a large extent. Therefore, the molecular model may have some actual validity for this system. Making certain reasonable approximations for force constants[26] and the extent of the charge distribution[15] in the excited state relative to that of the ground state, one may make an estimate of the ratio of $W_1$ to $W_3$ based upon the molecular model. One finds that this ratio should be about $\frac{4}{3}$, which is indeed quite close to that used in Fig. 10 for the CsI $F$ band.

The situation is quite different, however, in the other cesium halides where one expects the negative as well as the positive ions to move by significant amounts. The in-phase motion of the alkalis and halogens gives the largest rms displacements of the ions and, therefore, the most important electron-vibrational interactions. The resulting difference between cubic and noncubic distortions caused by the halogen motion is illustrated in Fig. 15 for the $\Gamma_1$ and $\Gamma_3^{(Z)}$ displacements. In Fig. 15(A) one sees that both positive and negative charges move away from the cube faces in a cubic distortion and, hence, that the potential change produced by the positive ion displacements is partially canceled by that of the negative ions. In contrast, for the noncubic distortion shown in Fig. 15(B), the positive charges move in toward the $z$ axis and out away from the $x$ and $y$ axes while the negative charges move out along the $z$ axis and in along the $x$ and $y$ axes. Thus the potential caused by the motion of the alkali ions is enhanced by that arising from the halogen ion motion, rather than being diminished as for the $\Gamma_1$ distortions. The same enhancement occurs not only for the $\Gamma_3$ and $\Gamma_5$ interactions in the CsCl lattice, but also in the usual fcc lattice where it may, in fact, be even more pronounced because there are fewer first-neighbor positive ions and more second-neighbor negative ions. Since the degree of enhancement and cancellation depends upon the relative amplitude of the halogen vibrations as well as the extent of the $F$-center charge cloud, the observed decrease in $W_1$ relative to $W_3$ as one progresses from CsI to CsF is to be expected as the halogens become lighter and of smaller ionic radius.

Let us now consider salts that have a relatively light alkali ion. The KCl $F$ center, for example, has a spin-orbit splitting[12,13] less than 100 cm$^{-1}$ and a characteristic low-temperature linebreadth of about 800 cm$^{-1}$. The corresponding rms lattice interaction of 560 cm$^{-1}$ is larger than that of 400 cm$^{-1}$ used in Fig. 12 for CsCl, consistent with the lighter alkali. Under these conditions we may picture the electronic states as essentially $|x\rangle$, $|y\rangle$, and $|z\rangle$, diagonal in the strong cubic and tetragonal interactions and only slightly perturbed by the weak spin-orbit coupling. Thus, unless the system is also subject to very strong distortions of $\Gamma_5$ symmetry, no dynamic distortion effects should be observed and the behavior should be adequately described by a single effective-vibrational interaction resulting in a nearly Gaussian line shape as discussed by Lax. Kristofel' and Zavt arrive at similar conclusions for the $^1S_0 \rightarrow {}^3P_1$ transition of KCl:Tl.[32] On the other hand, if the halogen ions are of high atomic number and cause a dominant spin-orbit interaction, then one should be able to observe dynamic distortion effects, at least in the circular dichroism studies, regardless of the weight of the alkali. The recent experiments of Gareyte and Merle-D'Aubigné[33] on KI appear to verify this expectation quite satisfactorily. One would also expect to observe dynamic distortion effects in the rubidium halides, particularly RbF, although the results would not be as obvious as for the cesium halides.

## ACKNOWLEDGMENTS

The author wishes to acknowledge discussions during the early stages of this work with Professor D. Y. Smith who contributed many useful ideas. In particular Professor Smith suggested that the quasimolecular model could be viewed only as a device for deriving the symmetry properties of the electron-lattice interactions and showed explicitly that distortions of $\Gamma_5$ symmetry caused effects which, for certain properties of the $F$-center states, could be accounted for by simply modifying the strength of the $\Gamma_3$ interactions.

The early recognition of the importance of the noncubic vibrations by C. H. Henry and S. E. Schnatterly and Professor C. P. Slichter was essential in motivating

[32] That no structure is observed in the $Tl^{(+)}$ impurity band in KCl is attributed by Kristofel' and Zavt (Ref. 20) to the extensive broadening produced by $\Gamma_1$ vibrations. The considerations outlined above suggest that, if one can introduce the $Tl^{(+)}$ impurity into a host lattice where the next-nearest neighbors are much lighter than the nearest neighbors, the resulting decrease in the symmetric interactions and increase in the noncubic interactions may enable one to observe the predicted structure.

[33] J. Gareyte and Y. Merle-D'Aubigné (private communication); and Compt. Rend. **258**, 6393 (1964).

the present inquiry whether the same distortions also explain other effects. Further discussion with these colleagues has been equally enlightening. Professor Slichter has also made many helpful suggestions in the preparation of the manuscript.

J. Margerie of the University of Paris and Dr. Y. Merle-D'Aubigné of the Fourier Institute in Grenoble have generously provided additional information concerning circular dichroism properties of $F$ centers in materials which produce strong spin-orbit couplings, and Dr. J. Mort and Professor F. C. Brown have made the Faraday rotation results readily available.

The author is especially indebted to Professor D. W. Lynch of Iowa State University, who not only provided the CsI $F$-center data, but also permitted their use in this paper prior to their publication elsewhere.

*Note added in proof.* The details of the arguments of the final section concerning the role of the halogen ions in diminishing the cubic and enhancing the noncubic interactions are based on a point ion model for a two shell quasimolecule and, as such, are intended to be only illustrative. Alternatively one could, for example, assume that the lattice modes having the greatest effect on the real $F$-center system are optical modes which project onto the defect site out-of-phase alkali and halogen motions and that the repulsive exchange forces dominate the electron-vibrational interaction. The conclusions are the same in either case.

PHYSICAL REVIEW VOLUME 137, NUMBER 3A 1 FEBRUARY 1965

# Relation between Electron Spin Resonance and Nuclear Magnetic Resonance in Transition Metal Intermetallic Compounds

D. SHALTIEL,* A. C. GOSSARD, AND J. H. WERNICK
*Bell Telephone Laboratories, Murray Hill, New Jersey*
(Received 31 August 1964)

A single system of intermetallic compounds, $La_{1-x}Th_xRu_2$, has been found in which both the nuclear magnetic resonance of $^{139}La$ and the electron spin resonance of added Gd impurities can be observed. Both the NMR Knight shift and the ESR $g$ shift were measured and found to vary with composition $x$. Linear relationships between $g$ and $K$ and between $K$ and $x$ were found as composition and temperature were varied, from which the effective exchange between spins of the Gd $4f$ electrons and the $d$ electrons of the formula unit was found to be $-0.05$ eV. The variations in $g$ and $K$ also allowed the magnitudes of the several sources of magnetic susceptibilities of the compounds to be evaluated. $\chi_{6s}{}^{\text{spin}} \leq 0.07\times10^{-4}$ emu/mole, and $\chi_{5d}{}^{\text{spin}}$ varies from $2.0\times10^{-4}$ at 1.4°K to $1.0\times1.0^{-4}$ at 300°K in $LaRu_2$, while the field-induced temperature-independent orbital paramagnetism of the $d$ bands is less than $0.7\times10^{-4}$ emu/mole for the La site in $LaRu_2$ and between $1.8\times10^{-4}$ and $2.4\times10^{-4}$ emu/mole for the Ru site in $LaRu_2$. A reversal in sign of the temperature dependence of the NMR Knight shift as composition was varied is interpreted in terms of changes in the density of electronic states at the Fermi surface as Th is alloyed in place of La.

THE electrons of metals interact both with nuclei in the metals undergoing nuclear magnetic resonance (NMR) and with electron ion core spins in the metals undergoing electron spin resonance (ESR). Previous work has demonstrated that a relationship exists between the magnetic susceptibility ($\chi$) and the Knight shift ($K$) of the frequency for NMR of transition metals,[1] alloys,[2] and the intermetallic compounds.[3] The behavior of $K$ and $\chi$ has been studied both as temperature was varied[1,3] and as the composition of alloys being studied was varied.[2] In the field for ESR as well ($H=h\nu/g\beta$), relationships between $g$ and $\chi$ have been found in metals,[4] alloys,[4] and intermetallic compounds.[5] We have now found a single system in which both the NMR $K$ and ESR $g$ shifts can be measured. It is the series of intermetallic compounds $La_{1-x}Th_xRu_2$.

The $La^{139}$ NMR was observed in eleven of these Laves phase compounds as a function of temperature, while the ESR of one mole percent Gd added as an impurity in place of La in compounds of the same composition was studied at 20°K. Earlier work had shown that the NMR $K$ and superconducting transition temperatures were sensitive functions of $x$ for $La_{1-x}Th_xRu_2$.[6] The ESR $g$ shift of Gd in this system now also is found to be sensitively dependent on $x$ and to vary with $K$ according to a unique linear relationship. The measure-

* Present address: Physics Department, Hebrew University, Jerusalem, Israel.

[1] A. M. Clogston, V. Jaccarino, and Y. Yafet, Phys. Rev. **134**, A650 (1964); J. A. Seitchik, A. C. Gossard, and V. Jaccarino (to be published).

[2] J. Butterworth, Proc. Phys. Soc. (London) **83**, 71 (1964).

[3] A. M. Clogston and V. Jaccarino, Phys. Rev. **121**, 1353 (1961); A. M. Clogston, A. C. Gossard, V. Jaccarino, and Y. Yafet, Phys. Rev. Letters **9**, 262 (1962).

[4] M. Peter, D. Shaltiel, J. H. Wernick, H. J. Williams, J. B. Mock, and R. C. Sherwood, Phys. Rev. **126**, 1345 (1962).

[5] D. Shaltiel, J. H. Wernick, H. J. Williams, and M. Peter, Phys. Rev. **135**, A1346 (1964).

[6] R. G. Shulman, B. G. Wyluda, and B. T. Matthias, Bull. Am. Phys. Soc. **6**, 103 (1961).